Astronomy & Astrophysics manuscript no. tf˙astroph March 20, 2008
(DOI: will be inserted by hand later)

arXiv:0803.3002v1 [astro-ph] 20 Mar 2008

IMAGES⋆-III: The evolution of the Near-Infrared Tully-Fisher relation over the last 6 Gyr

M. Puech[1,2], H. Flores[2], F. Hammer[2], Y. Yang[2], B. Neichel[2], M. Lehnert[2], L. Chemin[2], N. Nesvadba[2], B. Epinat[5], P. Amram[5], C. Balkowski[2], C. Cesarsky[1], H. Dannerbauer[6], S. di Serego Alighieri[7], I. Fuentes-Carrera[2], B. Guiderdoni[8], A. Kembhavi[3], Y. C. Liang[9], G. Östlin[10], L. Pozzetti[4], C. D. Ravikumar[11], A. Rawat[2,3], D. Vergani[12], J. Vernet[1], and H. Wozniak[8]

[1] ESO, Karl-Schwarzschild-Strasse 2, D-85748 Garching bei München, Germany
[2] GEPI, Observatoire de Paris, CNRS, University Paris Diderot; 5 Place Jules Janssen, 92190 Meudon, France
[3] Inter-University Centre for Astronomy and Astrophysics, Post Bag 4, Ganeshkhind, Pune 411007, India
[4] INAF - Osservatorio Astronomico di Bologna, via Ranzani 1, 40127 Bologna, Italy
[5] Laboratoire d'Astrophysique de Marseille, Observatoire Astronomique de Marseille-Provence, 2 Place Le Verrier, 13248 Marseille, France
[6] MPIA, Königstuhl 17, D-69117 Heidelberg, Germany
[7] INAF, Osservatorio Astrofisico di Arcetri, Largo Enrico Fermi 5, I-50125, Florence, Italy
[8] Centre de Recherche Astronomique de Lyon, 9 Avenue Charles André, 69561 Saint-Genis-Laval Cedex, France
[9] National Astronomical Observatories, Chinese Academy of Sciences, 20A Datun Road, Chaoyang District, Beijing 100012, PR China
[10] Stockholm Observatory, AlbaNova University Center, Stockholms Center for Physics, Astronomy and Biotechnology, Roslagstullsbacken 21, 10691 Stockholm, Sweden
[11] Department of Physics, University of Calicut, Kerala 673635, India
[12] IASF-INAF - via Bassini 15, I-20133, Milano, Italy

Received .....; accepted .....

Abstract. Using the multi-integral field spectrograph GIRAFFE at VLT, we have derived the K-band Tully-Fisher relation (TFR) at $z \sim 0.6$ in a representative sample of 65 galaxies with emission lines (W_0(OII) $\geq$ 15Å). We confirm that the scatter of the $z \sim 0.6$ TFR is caused by galaxies with anomalous kinematics, and find a positive and strong correlation between the complexity of the kinematics and the scatter contributed to the TFR. Once restricted to relaxed rotating disks, the TFR seems to not have evolved in scatter, and possibly in slope, while we detect an evolution of the K-band TFR zero point between $z \sim 0.6$ and $z = 0$. If interpreted as an evolution of K-band luminosity in rotating disks, they are brightening by 0.66 ± 0.14 mag from $z \sim 0.6$ to $z = 0$. Differences with Flores et al. (2006) are attributed to both the improvement of the local TFR and the more detailed determination of the rotation velocities in the distant sample. Most of the uncertainties can be attributed to the influence of the relatively coarse spatial resolution on the kinematical measurements. Because most rotating disks at $z \sim 0.6$ are unlikely to experience further merging events, one may assume that their rotational velocity (taken as a proxy of the total mass) would not evolve dramatically. If true, our result means that rotating disks observed at $z \sim 0.6$ are transforming rapidly their gas into stars, in order to roughly double their stellar masses to reach the TFR at $z = 0$. Indeed the selected rotating disks have emission lines and are either star-bursts or LIRGs, meaning they are forming stars at high rates. Thus, a significant part of rotating disks are actively forming the bulk of their stars within 6 to 8 Gyr, in good agreement with former studies on the evolution of the mass-metallicity relationship.

Key words. Galaxies: evolution; Galaxies: kinematics and dynamics; Galaxies: high-redshifts; galaxies: general; galaxies: interactions; galaxies: spiral.

1. Introduction

Since the first rotation curves obtained at intermediate redshifts (Vogt et al. 1993), a lot of work has been devoted to the evolution of the Tully-Fisher Relation (TFR, Tully & Fisher 1977), given its prominent role in constraining galaxy formation models (e.g., Dutton et al. 2007). First studies using the B-band found only modest luminosity evolution (Vogt et al. 1996, 1997), but subsequent studies in the same band have suggested a more significant evolution (Simard & Pritchet 1998;

Send offprint requests to: mpuech@eso.org

⋆ Intermediate MAss Galaxy Evolution Sequence, ESO programs 174.B-0328(A), 174.B-0328(E)

Bamford et al. 2006; Weiner et al. 2006; Chiu et al. 2007). In almost all these studies, the B-band TFR shows a very large dispersion in comparison with the local relation, especially at the low-luminosity (or velocity) end (e.g., Böhm et al. 2004). Böhm & Ziegler (2007) have recently shown that this effect could be attributed to incompleteness in magnitude provided that the scatter decreases by a factor of at least three between $z \sim 0.5$ and $z = 0$, with no evolution in slope or zero point. Alternatively, they have also proposed a possible luminosity-dependent evolution, with distant low-luminosity galaxies having lower mass-to-light ratios $[M/L]$ than their local counterparts, while higher-luminosity galaxies would not undergo strong M/L evolution. Therefore, the situation in B-band still remains unclear, particularly concerning the large scatter found at high redshift.

To minimize observational biases and favor comparisons with models, a progressive interest has been devoted to the K-band and stellar-mass TFRs (hereafter, smTFR). Long-slit spectroscopy of distant galaxies revealed a very scattered smTFR, with no detectable evolution neither in zero point nor in slope, up to $z \sim 1$ (Conselice et al. 2005). This much larger dispersion seems to be linked with "kinematically anomalous galaxies", as has been inferred from local studies (Kannappan & Barton 2004), or, from a morphological point of view, with disturbed, compact, or merging galaxies (Kassin et al. 2007; Atkinson et al. 2007). Noteworthy, Weiner et al. (2006) and Kassin et al. (2007) have defined a new tracer of the galaxy dark halo potential called S, which corrects the rotation velocity for disorded, non-circular motions. Once expressed using this new kinematical estimator, the distant smTFR shows a significantly reduced scatter, with no detectable evolution in zero point or in slope. This suggests an important role of non-ordered motions in increasing the scatter of the distant TFR.

In this respect, 3D spectroscopy provides us with a unique way to distinguish relaxed rotating disks from other kinematically disturbed galaxies. Kinematically-selected relaxed (or pure) rotating disks at $z \sim 0.6$ present a TFR that does not seem to evolve neither in slope, zero point, nor *dispersion* (Flores et al. 2006): kinematically anomalous galaxies (ranging from perturbed rotators where a rotation can still be detected to galaxies having complex kinematics with no noticeable rotation) seem to be responsible for the enlarged scatter of the distant TFR. Therefore, 3D spectroscopy allows us to establish a direct connection between non-ordered motions and kinematical and morphological anomalies. In this paper, we double the sample (see Yang et al. 2007, hereafter Paper I) to put on firmer grounds the results obtained in Flores et al. (2006).

This paper is organized as follows: Sect. 2 introduces the data used in this study; Sect. 3 details the methodology used for the analysis; Sect. 4 presents the K-band TFR obtained from GIRAFFE data, and Sect. 5 draw the conclusions from this work. In two appendixes, we derive the K-band luminosity density and the stellar-mass TFR in the GIRAFFE sample. Throughout, we adopt $H_0 = 70$ km/s/Mpc, $\Omega_M = 0.3$, and $\Omega_\Lambda = 0.7$, and the *AB* magnitude system.

2. Data

2.1. Distant sample

2.1.1. Kinematics

We used the multi-object integral field spectrograph FLAMES-GIRAFFE at VLT, to obtain the [OII] spatially resolved kinematics of a sample of 68 galaxies at $0.4 \leq z \leq 0.75$. The median redshift of the sample is $z_{med} \sim 0.61$, which corresponds to a look-back time ~ 5.8 Gyr, while the 25 and 75 percentiles of the redshift distribution are $z_{25} \sim 0.49$ and $z_{75} \sim 0.67$. This sample represents well the luminosity function of $z \sim 0.6$ galaxies with stellar masses $[M_{stellar}]$ in the $1.5 - 15{\times}10^{10} M_\odot$ range, and is also unaffected by field-to-field variations within Poisson statistics, as targets have been observed in four different fields (see Paper I).

Flores et al. (2006) and Paper I used GIRAFFE velocity fields [VF] and velocity dispersion maps [σ-maps], to define three kinematical classes, namely the *rotating disks* [RD], which correspond to relaxed rotators, the *perturbed rotators* [PR], corresponding to rotating disks showing some weak disturbances, and *kinematically complex* [CK] galaxies, corresponding to dynamically non-relaxed galaxies, likely associated with major mergers (see also Puech et al. 2006, 2007). This classification takes into account the residuals between the observed VF and σ-map and those predicted by a rotating disk model (see Paper I), which mitigates the subjectivity of a fully visual classification.

2.1.2. Morphology

A detailed morphological analysis of a sub-sample of 52 galaxies having multi-band HST/ACS imaging has been carried out by Neichel et al. (2008) (hereafter, Paper II). They find a good agreement between both kinematical and morphological classifications. Noteworthy, only 16% of galaxies in this sub-sample are both kinematically classified as RDs and morphologically classified as spirals. These "rotating spiral disks" have been selected as having a redder bulge than the disk and are therefore quite similar to local spirals, except their much bluer integrated colors and [OII] equivalent widths (see Paper II for a detailed discussion). Furthermore, they show no special trend in size nor in Bulge-to-Total luminosity ratio $[B/T]$ compared to local galaxies, and thus we do not expect any bias in the distant TFR that could be due to morphological variation of the TFR along the Hubble Sequence (see, e.g., Russell 2004). In the following, we will use the inclinations $[i]$ and half light radii $[R_{half}]$ as derived in Paper II.

The comparison between kinematics and morphology revealed two very special cases among RDs. First, J033230.78-275455.0 was detected in emission only on one half of the galaxy, which was due to a difficulty to correct for the superimposition of a sky line with the [OII] emission line. This galaxy was nonetheless successfully classified as a RD, but the amplitude of its VF is obviously affected by a very large uncertainty. Second, J033241.88-274853.9 was classified as a Tadpole galaxy in Paper II because of its highly asymmetric shape. In the following (see Sect. 3.2), we will assume that all

RD flux distributions can be reasonably well approximated by an exponential disk, which, obviously, does not apply to this galaxy. Therefore, in this paper, "RDs" will refer to galaxies classified as rotating disks by Paper I *excluding* J033230.78-275455.0 and J033241.88-274853.9, while "RD+" will refer to all RDs *including* J033230.78-275455.0 and J033241.88-274853.9.

2.1.3. Absolute K-band magnitudes

Absolute K-band magnitudes M_K were taken from Flores et al. (2006) and Ravikumar et al. (2007). They were derived using Bruzual & Charlot 2001 stellar population models, assuming a CSP template with solar metallicity and an exponential star formation history with $\tau = 0.5$ Gyr, which can fit most galaxies between $z = 0.4$ and 1 (Hammer et al. 2001). For each galaxy, an optimal SED was found matching the observed J-K color. This method was preferred to a full SED fitting because half of the sample (i.e., galaxies selected in the CFRS and the HDFS) do not have as many multi-wavelength photometric measurements as galaxies in the other half (i.e., those selected in the CDFS): using this technique would therefore not lead to homogeneous M_K estimates.

We compared, for galaxies on the CDFS, the impact of this simple "color-matching" method relatively to a full SED fitting (using optical photometry only): we find an excellent agreement between J-band absolute magnitudes with a $1-\sigma$ dispersion ~ 0.01 mag, and no systematic effect (Hammer & Pozzetti, private communication). We compared absolute J-band and not K-band magnitudes because whatever the method used, they are not extrapolations. Indeed, a potential drawback of the "color-matching" method is that M_K are extrapolated, since the reddest photometric point used is the observed K-band, which roughly falls in the middle of the rest-frame J and H band at $z \sim 0.6$. For galaxies in the CDFS, IRAC 3.6μm fluxes are publicly available, which allows us to compare the M_K obtained using this method with those obtained taking into account the IR 3.6μm flux: we find a residual $1-\sigma$ dispersion of 0.12 mag between both estimates, with no systematic effect. Moreover, using two independent photometric data sets for galaxies in the CDFS (i.e., EIS and ACS), we derived a random uncertainty $\lesssim 0.2$ mag on M_K, with no noticeable systematic uncertainties. Therefore, we adopted a random uncertainty of 0.2 mag and neglected systematic uncertainties.

Absolute magnitudes were corrected for internal extinction, using the mass-dependent method of Tully et al. (1998). We also applied an additional correction of 0.04 mag that accounts for extinction in face-on galaxies (Tully et al. 1998, 1985). Note that among the sample of 68 objects, three do not have available NIR photometry (see Tab. 1).

2.1.4. Summary

For the distant sample, all the measurements used in this paper are listed in Tab. 1. The columns of this table are as follows: (1) IAU ID, (2) Internal ID (the last 36 galaxies are in the CDFS), (3) Redshift z, (4) Inclination i (in deg., ±5 deg, see Sect. 2.1.2), (5) Dynamical Class D.C., (6) Projected radial velocity $\Delta V_{obs} \sin(i)$ (in km/s, see Sect. 3.1), (7) Rotation velocity corrected for inclination and spatial resolution effects V_{flat} (in km/s, see Sect. 3.1), (8) Total uncertainty on V_{flat} (in km/s, see Sect. 3.4), (9) Absolute K-band magnitude M_K (uncorrected for extinction), (10) Absolute K-band magnitude M_K^c corrected for extinction (±0.2 mag, see Sect. 2.1.3), and (11) Stellar-mass in $\log(M_{stellar}/M_\odot)$ (±0.3 dex, see Appendix A).

2.2. Local sample

In this study, we adopt as a local reference the K-band TFR derived by Hammer et al. (2007) from a complete sub-sample of the SDSS (Pizagno et al. 2007), which allows us to control systematics effects that could occur when comparing the local and distant samples.

One important choice for studying the TFR is the kinematical estimator used for the rotation velocity V_{rot}. Studies of the local TFR have shown that using different estimators (e.g., the maximal rotation velocity V_{max}, the plateau rotation curve velocity V_{flat}, the velocity measured at the radius containing 80% of the light V_{80}, the velocity $V_{2.2}$ measured at 2.2 disk scale length, etc.) can lead to different results (see, e.g., Verheijen 2001; Pizagno et al. 2007). V_{flat} has been shown to be a very good proxy of V_{rot}, since it is less influenced by the bulge dynamics (which can result in a central "bump" with $V_{max} > V_{flat}$): it leads to a tighter TF relation (e.g., Verheijen 2001), and improves significantly the linearity of the K-band relation at the high-mass end (Noordermeer & Verheijen 2007). For the local sample, we adopted the V_{80} measurements of (Pizagno et al. 2007) using arctan fits to the RCs. To limit uncertainties, we restricted the local sample to galaxies for which V_{80} is a good proxy for V_{flat} (i.e., Pizagno et al. 2007 flags 1 and 2), as shown by Hammer et al. (2007).

Rotation velocities were corrected for inclination using estimates derived from their morphological axis ratio. When well-resolved 2D kinematics is available, it is possible to derive the inclination directly from the fit of the VF. However, large differences (up to ~ 10 deg) can be found between such kinematically derived inclinations and the ones inferred from the morphological axis ratio (e.g., Chemin et al. 2006). Since we do not have 2D kinematics for galaxies in the local sample, we use morphologically-derived inclinations exclusively. Doing so provides us with a homogeneous estimates in the local and distant samples, since in the latter we will also use such inclinations.

Hammer et al. (2007) combined the Pizagno et al. (2007) kinematic measurements with 2MASS Ks photometry. We estimated absolute magnitudes in the local sample following the same method used in the distant sample, including corrections for extinctions (see Sect. 2.1.3). Of note, the 2MASS Ks filter has the advantage of being very close to the ISAAC Ks filter used in the distant sample. Indeed, both filters match very well the K-band LCO filter designed to establish the faint IR standard star system of Persson et al. (1998) (Mason et al. 2007; Carpenter 2001). We thus assumed that both filters are identical during the SED fitting procedure, which does not intro-

Table 1. Principle properties of the sample of 68 galaxies used in this study, ordered by increasing *RA* (see text).

IAU ID	Internal ID	z	i	D.C.	$\Delta V_{obs} \sin(i)$	V_{flat}	ΔV_{flat}	M_K	M_K^c	$\log(M_{stellar}/M_\odot)$
J030225.28+001325.1	CFRS030085	0.6100	71	RD	127	170	23	-20.83	-20.98	10.21
J030228.72+001333.9	CFRS030046	0.5120	66	RD	148	200	29	-21.68	-21.82	10.64
J030232.16+000639.1	CFRS039003	0.6189	29	RD	110	290	79	99.99	99.99	99.99
J030238.74+000611.5	CFRS031032	0.6180	37	PR	83	200	36	-22.64	-22.70	11.00
J030239.38+001327.1	CFRS030523	0.6508	41	CK	63	130	38	-21.55	-21.61	10.48
J030240.45+001359.4	CFRS030508	0.4642	38	CK	47	100	40	-20.34	-20.40	10.00
J030240.99+000655.4	CFRS031016	0.7054	67	CK	15	30	25	-21.24	-21.25	10.37
J030242.19+001324.3	CFRS030488	0.6069	41	CK	36	70	36	-20.84	-20.89	10.20
J030245.67+001027.9	CFRS030645	0.5275	45	CK	89	150	38	-21.34	-21.42	10.40
J030246.94+001032.6	CFRS030619	0.4854	27	RD	70	210	76	-21.93	-21.99	10.63
J030248.41+000916.5	CFRS031353	0.6340	57	RD	174	260	41	-22.42	-22.54	10.85
J030249.10+001002.1	CFRS031349	0.6155	48	PR	175	290	46	-22.92	-23.01	11.04
J030252.03+001033.4	CFRS031309	0.6170	71	CK	84	150	22	-22.91	-23.05	11.03
J033210.25-274819.5	4301297	0.6100	69	PR	110	150	26	-20.83	-20.96	10.29
J033210.76-274234.6	4402679	0.4180	26	CK	186	550	123	-23.62	-23.68	11.44
J033212.39-274353.6	3400803	0.4230	90	RD	105	180	22	-21.55	-21.85	10.61
J033213.06-274204.8	3500001	0.4220	79	CK	90	130	22	-20.56	-20.73	10.19
J033214.97-275005.5	3300063	0.6680	22	PR	62	190	90	-22.45	-22.50	10.92
J033217.62-274257.4	3401109	0.6470	46	CK	131	250	43	-21.15	-21.24	10.38
J033219.32-274514.0	3400329	0.7250	72	CK	116	270	29	-21.16	-21.36	10.39
J033219.61-274831.0	3300651	0.6710	49	PR	82	190	33	-20.90	-20.98	10.27
J033219.68-275023.6	3202670	0.5610	58	RD	161	230	33	-22.30	-21.42	10.88
J033220.48-275143.9	3202141	0.6790	63	CK	39	70	24	-20.63	-20.70	10.18
J033224.60-274428.1	3400618	0.5380	65	CK	63	90	27	-20.35	-20.44	10.08
J033225.26-274524.0	3400279	0.6660	60	CK	47	80	26	-21.54	-21.61	10.56
J033226.23-274222.8	3401338	0.6679	76	PR	150	200	24	-21.93	-22.13	10.72
J033227.07-274404.7	3400743	0.7390	84	CK	71	110	21	-20.95	-21.15	10.26
J033228.48-274826.6	3300684	0.6697	22	CK	23	130	66	-21.68	-21.73	10.63
J033230.43-275304.0	2200433	0.6460	70	CK	219	380	29	-21.68	-21.90	10.64
J033230.57-274518.2	2400243	0.6810	34	CK	41	80	46	-22.86	-22.91	11.08
J033230.78-275455.0	2102060	0.6870	66	RD+	90	200	43	-21.82	-21.96	10.66
J033231.58-274121.6	2500322	0.7047	42	RD	81	140	41	-20.51	-20.57	10.10
J033232.96-274106.8	2500425	0.4690	16	PR	31	210	117	-20.13	-20.17	10.01
J033233.90-274237.9	2401349	0.6190	17	PR	46	200	107	-21.82	-21.96	10.66
J033234.04-275009.7	2300055	0.7030	59	RD	104	160	29	-20.50	-20.60	10.09
J033234.12-273953.5	2500971	0.6280	32	CK	25	110	44	99.99	99.99	99.99
J033237.54-274838.9	2300477	0.6650	31	RD	106	230	71	-21.98	-22.03	10.70
J033238.60-274631.4	2301047	0.6220	60	RD	118	210	33	-21.45	-21.57	10.53
J033239.04-274132.4	2500233	0.7330	43	PR	58	130	39	-20.62	-20.68	10.14
J033239.72-275154.7	2200829	0.4160	35	CK	16	30	36	-20.94	-20.98	10.31
J033240.04-274418.6	2400536	0.5223	16	CK	108	470	214	-21.95	-22.00	10.77
J033241.88-274853.9	2300404	0.6680	67	RD+	80	120	27	-20.90	-21.01	10.27
J033243.62-275232.6	2200611	0.6800	71	PR	38	60	23	-19.94	-20.01	9.86
J033244.20-274733.5	2300750	0.7365	39	CK	46	170	40	-21.76	-21.83	10.62
J033245.11-274724.0	2300800	0.4360	43	RD	95	270	44	-22.03	-22.11	10.80
J033248.28-275028.9	1202537	0.4462	81	PR	76	110	22	-20.38	-20.54	10.09
J033249.53-274630.0	1302369	0.5230	46	PR	74	150	39	-21.00	-21.07	10.34
J033250.24-274538.9	1400714	0.7318	31	CK	82	240	67	-20.59	-20.65	10.12
J033250.53-274800.7	1301018	0.7370	62	PR	71	110	26	-20.34	-20.43	10.01
J221741.46+001854.8	CFRS221119	0.5138	41	RD	135	250	47	99.99	99.99	99.99
J221743.08+001508.3	CFRS221064	0.5383	48	PR	93	250	29	-21.64	-22.74	10.53
J221745.12+001447.4	CFRS220975	0.4211	50	CK	313	410	44	-22.53	-22.64	10.95
J221746.48+001653.5	CFRS220919	0.4738	60	CK	39	30	23	-19.53	-19.55	9.67
J221754.56+001900.3	CFRS220619	0.4676	68	PR	62	90	24	-19.33	-19.42	9.63
J221758.07+002137.5	CFRS220504	0.5379	42	RD	93	170	42	-21.36	-21.43	10.43
J221802.92+001428.0	CFRS220321	0.4230	42	PR	104	220	46	-20.79	-20.87	10.21
J221803.55+002131.9	CFRS220293	0.5420	45	CK	89	160	40	-20.89	-20.97	10.24
J223241.45-603516.1	HDFS4130	0.4054	36	CK	90	220	53	-22.13	-22.20	10.76
J223245.56-603418.8	HDFS4170	0.4602	51	RD	134	230	37	-22.60	-22.70	10.96
J223252.74-603207.3	HDFS4040	0.4650	51	PR	75	120	32	-20.04	-20.11	9.88
J223254.05-603251.6	HDFS4090	0.5162	45	CK	14	20	30	-19.83	-19.85	9.80
J223256.07-603148.8	HDFS4020	0.5138	50	RD	88	140	36	-20.12	-20.20	9.96
J223256.08-603414.1	HDFS5140	0.5649	50	CK	171	220	42	-20.46	-20.56	10.04
J223257.52-603305.9	HDFS5030	0.5821	25	CK	31	130	69	-22.68	-22.73	10.94
J223258.01-603525.9	HDFS4180	0.4647	64	RD	104	140	26	-20.38	-20.49	10.04

duce any systematic effect. Note than 2MASS K-band magnitudes were converted into AB magnitudes using $Ks(AB) = Ks(Vega) + 1.85$, following Blanton et al. (2005).

Since we are exploring the higher tail of the stellar mass regime and that the TFR is highly sensitive to the stellar mass involved (see, e.g., McGaugh 2005), we restrict the K-band TFR to $\log(V_{flat}) \geq 2.2$ and find (Hammer et al. 2007):

$$M_K(AB) = -6.54 \pm 1.33 - (6.88 \pm 0.57) \times \log(V_{flat}), \quad (1)$$

with a residual dispersion $\sigma_{res} = 0.38$ mag. Because we use uniform M_K error-bars, we used direct fits to the TFR, i.e., with M_K as a V_{flat}-dependent variable (using the IDL MPFITFUN procedure of C. Markwardt, translated from the MINPACK-1 package[1]).

3. Methodology

3.1. Derivation of the rotation velocity

For each galaxy, we estimated the de-projected VF half-amplitude using $\Delta V_{obs} = (V^{IFU}_{max} - V^{IFU}_{min})/(2\sin(i))$, where V^{IFU}_{max} and V^{IFU}_{min} are respectively the maximal and minimal values of the VF sampled by the IFU (see Tab. 1).

Because of the influence of the seeing, ΔV_{obs} underestimates the true rotation velocity V_{rot} (see Flores et al. 2006; Puech et al. 2006). Rather than applying a mean correction factor to the whole sample as in Flores et al. (2006), we now correct *individually* each galaxy by modeling its data-cube. To do so, we used a method derived from the one used in Flores et al. (2006) and Paper I to model the σ-map. Assuming that all galaxies are thin rotating disks, it is possible to model their data-cube from their observed VF and σ-map in the following way.

First, for each galaxy, we constructed a grid of rotation curves (RC) with V_{rot} spaced by 10 km/s, which roughly corresponds to the typical uncertainty on ΔV_{obs} (see Sect. 3.4). Because of a lack of spatial resolution, the precise shape of distant RCs remains largely unknown. Therefore, we chose a simple arctan defined as $V_0 \times (2/\pi) \times \arctan(r/r_t)$, which depends only on two parameters, i.e., the asymptotic velocity V_0, and the "turnover" radius r_t (see, e.g., Courteau 1997). This RC shape has been used in Paper I to model the VF of each distant galaxy. In the RD+ sub-sample, such models provide very good matches to the observed VFs, which shows that such a RC shape is a reasonable choice. Moreover, the same shape was adopted in the local sample (see Sect. 2.2), which provides us with homogeneous estimates of the rotation velocity in both the local and distant samples. We chose not to fit a wide range of values for r_t because a visual inspection of VFs reveals that in almost all RDs, the gradient of the RC falls within only one GIRAFFE IFU pixel (Flores et al. 2006, Paper I): we therefore explored only three fixed values for r_t (see Fig. 1), which nevertheless allows us to explore more extreme cases where the RC is relatively steep or, on the contrary, relatively flat.

The arctan RC model cannot reproduce the central "bump" seen in some early-type galaxies (see, e.g., Fig. 1). However,

[1] http://cow.physics.wisc.edu/ craigm/idl/mpfittut.html

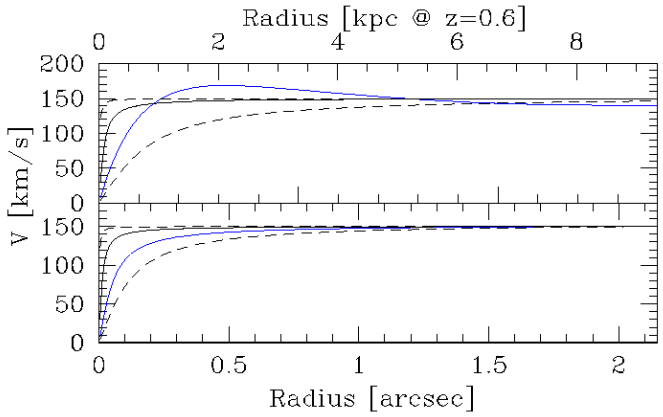

Fig. 1. Illustration of the ΔV_{obs} correction method, for an early-type RC (*upper panel*, note that $V_{max} > V_{flat}$) and a late-type RC (*bottom panel*). The blue thick curves represent the input RC of the test, the black curves the best models (see text), and the dash-lines the two alternative RCs with non-optimal r_t. Note that typical r_t values lead to velocity gradient on spatial scales much smaller than the typical seeing of ~ 0.8 arcsec.

given the relatively coarse spatial resolution of the GIRAFFE IFU (0.52 arcsec/pix, i.e., ~ 3.5 kpc at $z = 0.6$) and the large size of the seeing disk compared to the size of distant galaxies, it might be not possible to clearly distinguish between V_{max} or V_{flat} in distant galaxies: one might expect that the asymptotic velocity V_0 corresponding to an arctan RC is probably in this case an average value between V_{max} and V_{flat}. Because we rely on V_{flat} as a kinematic tracer for the rotation velocity in the local sample (see Sect. 2.2), we are nevertheless naturally led to quantify all random and systematic uncertainties relative to V_{flat}. Finally, note that even for late-type RCs, $V_0 \sim V_{flat}$ only if the RC has a well defined plateau and if this plateau can be observed in terms of spatial coverage or SNR.

From each RC, a high resolution data-cube was constructed, assuming a simple Gaussian shape for the emission line. For simplicity, we did not include noise in the simulations, assuming that the global uncertainty can be derived by estimating separately the influence of the noise and other effects (see Sect. 3.4). As a consequence, neglecting the doublet spectral nature of the [OII] emission line should not impact severally the results. The velocity width was assumed to be the minimal value observed in the σ-map, and the emission line flux was taken from an exponential flux distribution, assuming $R_d \sim R_{half}/1.6$ (Persic & Salucci 1991) and limiting the spatial extent to a radius $2R_{half} \sim 3R_d \sim R_{opt}$, where R_d is the disk scale-length, and R_{opt} is the optical radius. We chose to use R_{half} rather than direct R_d measurements because more than 80% of galaxies in the sample are not classified as simple spirals but have more complex morphologies (see Paper II), which could lead to meaningless R_d values. Instead, R_{half} provides us with a uniform and well-defined size-parameter, which can be safely converted into R_d for thin exponential disks: using the bulge/disk decomposition of the RD subsample done in Paper II, we compared R_d with $R_{half}/1.6$, and found a *maximal* difference of ~ 0.1 arcsec, which is much smaller than the typi-

cal seeing during the observations (see also Puech et al. 2007). Thus, such an error on R_d has very little influence on the model, and we chose not to explore this parameter.

Each high resolution data-cube was convolved by a 0.8 arcsec seeing, which roughly corresponds to the median condition of the observations, and was then re-binned at the GIRAFFE sampling, i.e., 0.52 arcsec/pix. From these simulated GIRAFFE data-cubes, simulated VFs and simulated ΔV_{model} were derived as for real GIRAFFE data. We checked the influence of changing the seeing value from 0.8 to 1.0 arcsec on ΔV_{model}: using Monte-Carlo simulations of 100 GIRAFFE data-cubes (see next section), we found a very good linear correlation between the ΔV_{model} obtained with a 1 arcsec seeing and the one obtained with a 0.8 arcsec seeing (all else equal). This fit indicates that with a 1 arcsec seeing, ΔV_{model} is reduced by $\sim 0.05\%$ compared to the one obtained with a 0.8 arcsec seeing (see Fig. 2). Therefore, the maximal uncertainty on ΔV_{model} due to seeing variations is ~ 12 km/s, which roughly corresponds to the velocity spacing adopted for the searching grid used to correct ΔV_{obs} (see above), meaning that this velocity grid is relatively well adapted to our purpose.

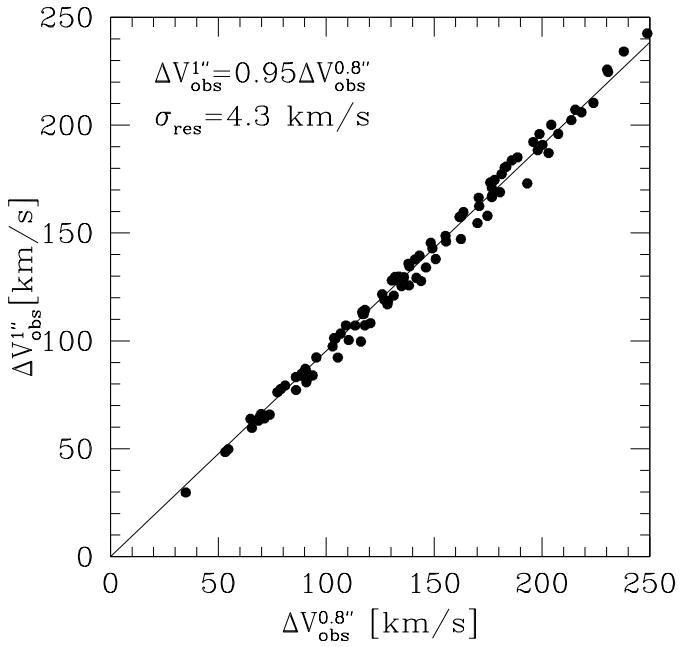

Fig. 2. Comparison between the ΔV_{model} values obtained in Monte-Carlo simulations of 100 GIRAFFE data-cubes using a 0.8 and 1 arcsec seeing (see text). The black line is a linear fit fixing the intercept to zero. The residual dispersion is ~ 4.3 km/s.

Finally, to find the best model, we simply looked for the (r_t,V_{flat}) pair minimizing the difference between ΔV_{model} and ΔV_{obs}. We checked that, in all simulations, such a criterion gives a unique solution. Results are listed in Tab. 1, and examples of such a kinematical fitting for three RD galaxies are shown in Fig. 3.

3.2. Testing the method of correction

To test this method of correction, we used Monte-Carlo simulations of 100 GIRAFFE data-cubes. The parameter space investigated encompasses the inclination, half-light radius, *PA*, rotation velocity, and RC gradient: these values are randomly chosen in the typical range of values observed in the GIRAFFE sample. Half of them were generated using an arctan RC shape model, and the other half using an exponential term combined with a second order polynomial term. This polynomial part allows us to create a central velocity "bump" as observed in early-type galaxies (see Fig. 1). Note that for late-type RCs, we did not require that V_{flat} be located within the IFU, which allows us to simply test how the correction procedure operates in this case. For early-type galaxies, V_{flat} should be located within the IFU, as generally V_{max} is located close to $2.2R_d \sim 1.375R_{half}$ (e.g., Courteau 1997), which almost always falls within the IFU (Flores et al. 2006). Note, however, that in some cases, because of the dynamical influence of the bulge, the RC of some early-type galaxies can show an extended velocity peak up to large distances (see, e.g., M31, Carignan et al. 2006). In this case, the limited spatial coverage of the GIRAFFE IFU would probably provide us with an overestimation of the rotation velocity. In the RD sample, all but one galaxy have $B/T < 0.2$, which means that such an effect cannot affect significantly the RD sample.

These simulated RCs were used to simulate GIRAFFE observations following the method outlined in Sect. 3.2. These simulated data-cubes were in turn used as inputs to test the method of correction on ΔV_{obs}. In Fig. 4, we compare the input rotation velocity V_{flat}, with the asymptotic velocity V_0 of the best arctan model obtained using the method detailed above. We find a good linear correlation with $V_0 = [0.65 \pm 6.22] + [1.00 \pm 0.03]V_{flat}$, consistent with $V_0 = V_{flat}$, and a residual dispersion ~ 17 km/s. In this figure, we have distinguished between simulations where V_{flat} is sampled by the IFU (black circles) from those where this is not the case (black squares). If we compare the corrected velocity V_0 with the last point of the RC sampled by the IFU V_{end}, both sets of simulations then falls on the same region. In such a plot (not shown here), we find a similar result, with $V_0 = [-1.23 \pm 4.47] + [1.03 \pm 0.02]V_{end}$, also consistent with $V_0 = V_{end}$.

We checked that r_t has little influence on the ΔV_{obs} correction by comparing the corrected rotation velocity obtained letting r_t vary among the three values defined in Sect. 3.2 (as above), with that obtained fixing r_t to the middle value of this grid, i.e. the one which makes most of the RC gradient fall in one GIRAFFE pixel as observed in most cases. We found that both sets of values correlate well within ~ 6 km/s ($1-\sigma$), i.e., as expected, r_t has a negligible impact on the derived correction. This is mainly due to the large seeing size ($\sim$0.8 arcsec) compared to velocity gradients associated with typical r_t values (see Fig. 1), which largely dilutes variations of RC gradient, once projected onto the IFU.

One important point is to check whether or not these simulations are representative enough of real galaxies. To do this, we selected a few galaxies in the GHASP survey (Amram et al. 2002), which provides us with high spatial resolution data-

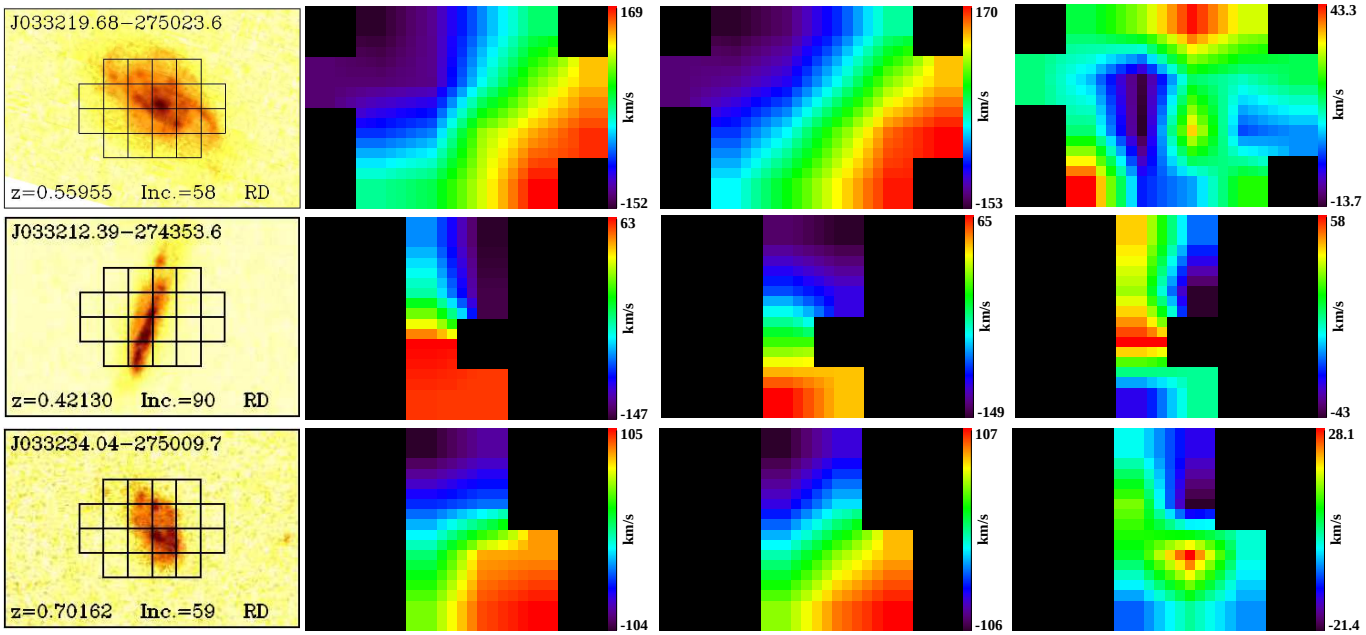

Fig. 3. Examples of kinematical fitting of three $z \sim 0.6$ RD galaxies. *From left to right:* HST/ACS F775W image with the GIRAFFE IFU superimposed (from Paper I), observed VF (shown with a 5x5 interpolation see Paper I), best modeled VF (shown with a 5x5 interpolation), residual map between the observed and modeled VFs. Relatively large differences are found only close to the minor axis, where departure from pure circular motion is artificially exaggerated by important projection effects (see a discussion of this effect in, e.g., (Chemin et al. 2006)).

cubes for a morphologically complete sample of local galaxies using Perot-Fabry interferometry. The analysis of the GHASP sample is still underway (Epinat et al. 2008), and a full comparison between local 3D data and distant 3D GIRAFFE data will be addressed in a future work. Here, we just want to check whether or not the simulations are representative enough of local galaxies, especially in the range of velocity and size spanned by distant RDs. In addition, we want to restrict our choice to galaxies for which an arctan shape provides us with a relatively good representation of the RC, as we only want to probe the accuracy on the correction applied on ΔV_{obs}, and not on the measurement itself, which is an independent issue. Given the limited number of galaxies meeting these criteria, we chose to restrict our choice to 7 such galaxies with rotation velocities ranging from 190 to 220 km/s, where most of distant RDs fall (see next Sect. 4). This choice allows us to roughly sample to most relevant velocity range for distant RDs, rather than testing a few isolated points spread over the full velocity range of the distant sample. We simulated GIRAFFE observations by degrading their Perot-Fabry high resolution data-cube to the resolution of GIRAFFE observation (0.8 arcsec seeing) and then to the GIRAFFE IFU spatial sampling. From these data-cubes, we extracted a VF and ΔV_{obs} as for real GIRAFFE data, and corrected them. These simulations are shown as blue stars on Fig. 4: these points are in agreement with the Monte-Carlo simulations that fall in the same velocity range, reproducing well the dispersion of the correlation. This confirms that we can confidently rely on the correction made on ΔV_{obs}.

We now plot in Fig. 5 all correction factors $\alpha = V_{flat}/\Delta V_{obs}$ obtained for the Monte-Carlo simulations. Both simulations of redshifted local galaxies and real GIRAFFE rotating disk galaxies fall in the same region of the plot, except three galaxies (J033212.39-274353.6, J033230.78-275455.0,J033245.11-274724.0), that show relatively large α. One is a compact galaxy (J033245.11-274724.0, see Paper II), while another one is seen almost edge-on (J033212.39-274353.6), which might explain their relatively high α. The last one (J033230.78-275455.0) is a very special case, as only half of the galaxy is detected in emission (this galaxy was shifted into the RD+ class in Sect. 2.1). We checked that the results presented in this paper are not significantly affected when these three special objects are removed from the sample. Finally, in the RD sub-sample, we find a median $\alpha \sim 1.26$, consistent with what is found in the Monte-Carlo simulations, with a mean $\alpha = 1.25 \pm 0.12$.

3.3. Random uncertainty budget of the rotation velocity derivation

The uncertainty budget can be decomposed into uncertainties related to ΔV_{obs}, and those related to the correction applied on ΔV_{obs} to obtain V_{flat}.

The main source of uncertainty that can affect ΔV_{obs} is the one associated to a finite spectroscopic SNR in the measurement of V_{max}^{IFU} and V_{min}^{IFU} , which can be quantified using Monte-Carlo simulations (see Fig. 6). For each galaxy, we used the SNR maps derived in Paper I to estimate the mean SNR uncertainty on V_{max}^{IFU} and V_{min}^{IFU}, i.e., on ΔV_{obs}. We found a median (mean) uncertainty due to a finite SNR of ∼9 km/s (8km/s).

We used Fig. 4 to quantify the uncertainty associated to the correction made on ΔV_{obs} (see Sect. 3.3). We found 17 km/s ($1-\sigma$ residual dispersion), with no noticeable systematic uncertainties. Notice that this uncertainty takes into account

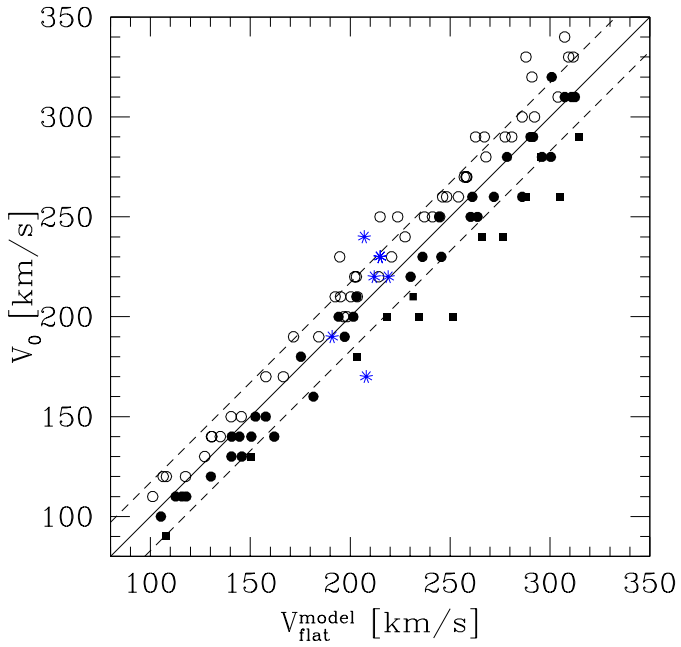

Fig. 4. Comparison between the V_{flat} used as inputs for the Monte-Carlo simulations of 100 GIRAFFE data-cubes, with the V_0 values obtained after using the method of correction described in Sect. 3.2. Black dots represent RCs generated using an arctan model (i.e., late-type like RCs), while open circles represent RCs typical of early-type galaxies. Black squares represent simulations where the rotation velocity is not sampled by the IFU (see text). The black line is a linear fit, and the dash lines represent the $1-\sigma$ residual dispersion ∼17 km/s. Blue stars represent real observations of local galaxies artificially redshifted to $z \sim 0.6$ (see text).

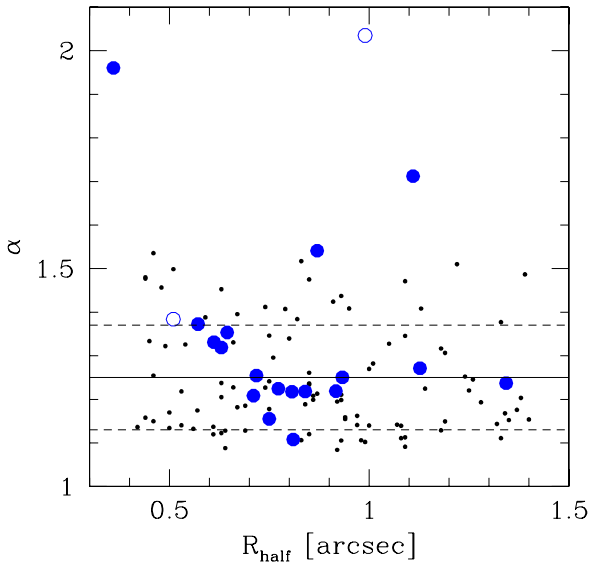

Fig. 5. Correction factors α used to correct ΔV_{obs} for RDs (blue dots; open blue dots represent the two RD+ galaxies). Small black dots correspond to Monte-Carlo simulations of 100 GIRAFFE data-cubes in the same range of half-light radius, PA, inclination, rotation velocity, and RC gradient (see text). The horizontal dash line represents to the mean correcting factor of 1.25 derived from Monte-Carlo simulations, wile the $1-\sigma$ dispersion around the mean is shown in dash lines.

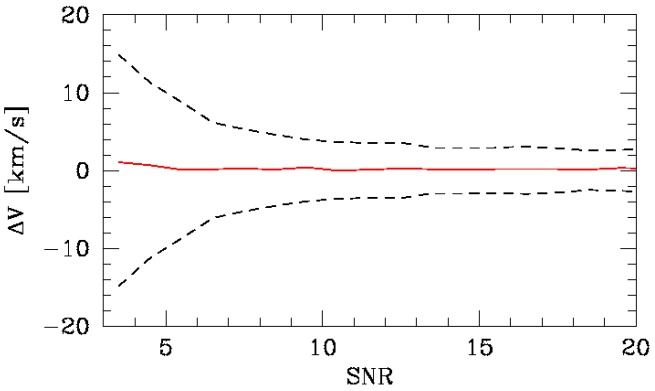

Fig. 6. Monte-Carlo simulations of the velocity measurement accuracy (see Paper I for details). The red line shows the corresponding bias (almost zero), while the black dashed lines shows the $1-\sigma$ error: ∼12 km/s between SNR=3-5, ∼5 km/s between SNR=5-10, and ≤ 2 for SNR≥10.

cases where the RC is not fully sampled by the IFU. As we have already pointed out, one very special case in the sample deserves more interest. For J033230.78-275455.0, which was classified as RD+ (see Sect. 2.1), only one part of the galaxy was detected in emission (see Paper I). Then, ΔV_{obs} does not encompass a symmetric range along the RC, biasing the rotation velocity input of the model to a lower value. Considering a rough RC model, composed of a first, linear, rising part up to $R_{max} = 2.2R_D$ (Persic & Salucci 1991), and a second flat part, we estimate a ∼30km/s correction to "symmetrize" ΔV_{obs}. This correction is directly convolved to the other uncertainty factors on ΔV_{obs}. Finally, following Sect. 3.3, we also took into account uncertainties due to seeing and r_t variations (∼5 and 6 km/s, respectively), which led us to a total uncertainty for the correction on ΔV_{obs} of ∼19 km/s.

The total uncertainty on V_{flat}×sin (i) (i.e., the radial rotation velocity uncorrected for inclination) was derived by adding in quadrature all the previous terms. We finally propagate the uncertainty associated with the inclination, which is ±5 degrees, according to Paper I. We finally found a median (mean) total uncertainty on V_{flat} of ∼37 km/s (44km/s). The $1-\sigma$ dispersion of the total uncertainties around the mean is ∼30 km/s.

4. The K-band Tully-Fisher relation at $z \sim 0.6$

4.1. Results

We compare both the distant and local K-band TFR in Fig. 7. Holding the slope to the local value, σ_{res} increases from RDs (0.31 mag), to PRs (0.80 mag) and CKs (2.08 mag). Restricting the distant TFR to dynamically well-relaxed RDs, the local and distant relations have comparable σ_{res}: we therefore confirm quantitatively the previous findings of Flores et al. (2006) that

all of the enlarged dispersion of the distant TFR comes from non-relaxed galaxies. If we let the slope free during the fit, we also find a residual dispersion of 0.31 mag. This indicates that assuming no evolution in slope seems to be a reasonable assumption.

The zero point of the TFR of distant RD galaxies is found to be -5.88 ± 0.09 ($1-\sigma$ bootstrapped error, slope fixed), i.e., 0.66 mag fainter that the local zero point. Moreover, letting the slope free during the fit, we find a zero point of -5.07 ± 2.37 and a slope of -7.24 ± 1.04 in agreement (within the corresponding uncertainties) with those derived fixing the slope to the local value. Again, this strongly suggests no evolution in slope of the K-band TFR. Given the limited number of RDs in the distant sample (16), in the following, we adopt the zero point value derived keeping the slope to the local value. Note that if we now consider the RD+ class (18 galaxies, see Sect. 2), we find very similar results (see Tab. 2).

We find in the distribution of M_K residuals, a skewness and a kurtosis of -0.22 and -0.99 respectively for RDs, which is roughly consistent with Gaussian residuals, within the $1-\sigma$ expected thresholds[2]. This indicates that residuals are not significantly biased on any side of the relation. A Welcher's t-test then gives a probability $\ll$1% that the local and distant relations have the same zero point. Notice that during the fitting procedure, we have weighted all the rotation velocities by their associated uncertainties. Therefore, the result of the Welcher's t-test means that within random uncertainties, the zero point difference of 0.66 mag between the distant and the local relations is statistically significant.

4.2. Systematic uncertainty budget

We now investigate which systematic effects could bias the evolution of zero point of the TFR detected between $z \sim 0.6$ and $z = 0$.

4.2.1. Photometric systematic uncertainty

As stated in Sect 2.4, we do not expect any noticeable systematic effect due to photometric measurement or calibration. However, one possible caveat is the extinction correction made on both local and distant galaxies. Even if we follow exactly the same procedure in the two samples, one might indeed wonder whether or not low surface brightness outer regions in distant galaxies could be lost compared to local galaxies, which would imply a bias in the derivation of their axis ratios and extinction corrections. However, we found in Paper II that the HST/ACS imaging used to derive the axis ratio in distant galaxies allows us to reach the optical radius ($\sim 3.2 \times R_d$), which limits such a bias. Moreover, notice that extinction corrections are relatively small in the K-band: in the distant sample, we find a mean/median correction of 0.11 ± 0.05 mag ($1-\sigma$ dispersion), while in the local sample, the mean (median) correction is found to be $0.15(0.14) \pm 0.05$, consistent one with each other within their respective uncertainties.

[2] For a distribution of n points, these thresholds are $\sqrt{(6/n)}$ and $\sqrt{(21/n)}$ respectively (n=16 is the present case).

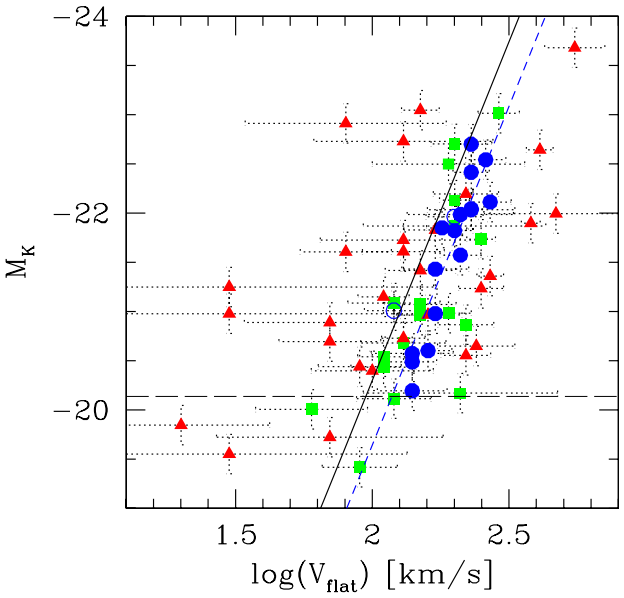

Fig. 7. Evolution of the K-band TFR (*AB* magnitudes). The completude limit $M_K \sim -20.14$ (corresponding to $M_J = -20.3$, see Sect. 2) is indicated by an horizontal dash line. Blue dots represent RDs (the two RD+ galaxies are represented with open blue dots), green squares PRs, and red triangles CK galaxies. The black line is the local TFR, while the blue dash-line represent a linear fit to the $z \sim 0.6$ TFR (see text).

4.2.2. Effects related to the comparison to the local relation

One important aspect about the evolution of the TFR is to control systematic effects between the distant and local relations. These considerations have led us to adopt as a local reference the TFR derived by Hammer et al. (2007) in a complete sub-sample of the SDSS (Pizagno et al. 2007) (see Sect. 2.2). However, there are several differences between the local and distant samples that could lead to possible biases when comparing the corresponding TFRs.

First, kinematical data are obtained using different techniques (3D spectroscopy vs. long-slit spectroscopy). We have mitigated this effect by restricting the local sample to galaxies having a well-defined RC (see details in Hammer et al. 2007). This also mitigates the assumption that both local and distant galaxies have RC shapes than can be well described by an arctan (see Sect. 2.2 and 3.2). Second, a different emission line is used for deriving the rotation velocity ([OII] and H_α). However, on overall, both emission lines are found to give similar estimates of the rotation velocity (e.g., Saintonge 2007). Third, in the local sample, V_{80} (defined as the velocity at a radius that encompasses 80% of the light) is used as a proxy for V_{flat}, while we directly used the asymptotic V_0 from the arctan RC in the distant sample. However, V_{80} is a very good proxy for V_{flat}, as shown in Hammer et al. (2007) (see also Pizagno et al. 2007). Finally, one possible caveat about the use of 2MASS K-band magnitudes was recently pointed

Table 2. Fits to the local and distant K-band TFRs, using $M_K(AB) = a + b \times \log(V_{flat})$.

K-band TFR	Slope a	Zero point b	Comments
Local relation	-6.88±0.57	-6.54±1.33	SDSS sub-sample
Distant RDs	-6.88	-5.88±0.09	Using local slope
Distant RDs	-7.24±1.04	-5.07±2.37	Slope free
Distant RD/RD+	-6.88	-5.92±0.10	Using local slope
Distant RD/RD+	-6.47±1.30	-6.85±2.98	Slope free

out by Noordermeer & Verheijen (2007), i.e. that 2MASS underestimates the K-band luminosity in relatively low surface brightness galaxies. Note that this bias would go in the opposite trend compared to the evolution seen in the TFRs, i.e., shifting the local relations towards brighter magnitudes or larger stellar masses. However, we have also mitigated this effect by restricting the local relation to galaxies having $Log(V_{flat}) \geq 2.2$, i.e. to the most massive galaxies (see Sect. 4.1).

4.2.3. Kinematic systematic uncertainty

In this study, we have restricted the analysis of the TFR evolution to well-relaxed RDs. Indeed, in distant TFR studies, it is often assumed that the (gas) rotation velocity can be simply derived as the half-amplitude of the VF divided by $\sin(i)$ (modulo spatial resolution effects): a very important assumption behind this simple prescription is that the azimuthal velocity component of the 3D velocity vector within the galaxy (i.e., the rotation) dominates its projection along the line-of-sight. Strictly speaking, this assumption should always be checked *a posteriori*, showing that residuals between a rotating disk model and the observed VF are small compared to the amplitude of rotation motions. In the case of GIRAFFE RDs, there are few doubts that this assumption is correct, as their modeled VFs match very well the observed ones (see Paper I).

Conversely, CK galaxies are clearly out of dynamical equilibrium (see Flores et al. 2006 and Paper I). As a consequence, one does no longer know which component of the 3D velocity vector dominates its projection along the line-of-sight. Actually, if these galaxies are truly associated with mergers as we will discuss below, deriving the rotation velocity in this way is probably very uncertain, if not meaningless. This is the reason why in this study, we have always restricted the analysis of the TFR to well-relaxed RDs.

In Sect. 3, we have extensively tested the method of correction used to correct ΔV_{obs} for spatial resolution effects. During the process all galaxies are assumed to be RDs, whatever their kinematical class is (see Puech et al. 2006, 2007). However, doing so provides us with uniform α values independent of the kinematical class: a misclassification of a galaxy has no impact on the way α is derived. This approach also helps to compare with long-slit spectroscopy results, where all galaxies are implicitly assumed to be RDs (e.g., Conselice et al. 2005). Moreover, as explained above, the fit to the TFR is restricted to RDs only, and therefore this cannot impact on the evolution of the zero point of the TFR.

One might wonder whether or not the slight bias found in Fig. 4 between early and late type galaxies could influence significantly the results. Once translated into $\log(V_{flat})$ (using Eq. 1), the offset of the distant TFR is found to be -0.1 dex between $z \sim 0.6$ and $z = 0$, which is much larger than the one found in Fig. 4 for early-type galaxies (∼0.025 dex). Moreover, late-type galaxies have the opposite trend, resulting in a -0.014 dex offset in Fig. 4. Then, it is impossible to explain all the shift of the distant TFR zero point in terms of such a morphological bias. Finally, looking at the TFR residuals against B/T for RDs that have been analyzed in Paper II, we find no special trend, which definitively excludes such a bias.

Another source of systematic uncertainty could come from the limited spatial coverage of the GIRAFFE IFU. Indeed, Fig. 4 (see the black squares) shows that when the plateau of the RC is not sampled by the IFU, the recovered rotation velocity is underestimated on average by ∼0.03 dex. Note that this effect generally lead to underestimate V_{flat}, which would contribute to increase the shift of zero point between the local and the distant TFRs. However, most of the RDs are well spatially covered by the IFU (see Flores et al. 2006 and Paper I), and this could only affect a few galaxies among the sample. It is thus unlikely that such an effect could affect significantly the results in a systematic way.

Finally, the most important possible systematic uncertainty likely comes from our limited knowledge of the seeing during observations. Individual variations from galaxy to galaxy leads to relatively small random uncertainties (see Sect. 3.2). However, we assumed a uniform value of 0.8 arcsec during the rotation velocity correction process. According to Fig. 2, changing the seeing in the simulations from 0.8 to 1.0 arcsec implies a systematic effect of -0.02 dex on the rotation velocity correction.

4.2.4. Total systematic uncertainty

The only possible systematic effect we can identify so far is the one associated to the kinematics (derivation of the correction for the rotation velocity). Using Eq. 1, this translates into a possible systematic uncertainty of ±0.14 mag on the 0.66 mag evolution of the K-band TFR zero point between $z \sim 0.6$ and $z = 0$, which represents 20% of the shift.

5. Discussion

5.1. Comparison with Flores et al. (2006)

In Flores et al. (2006) (see also Puech et al. 2007), we used hydro-dynamical simulations of an Sbc galaxy to infer a mean correction factor $\alpha = 1.2 \pm 0.05$ on V_{max} for galaxies having sizes between 2 and 3 arcsec, which is less that what we find

here in Monte-Carlo simulations. At first sight, it is quite surprising to find a larger mean α for V_{flat} than for V_{max} (since $V_{flat} \leq V_{max}$). The explanation for this is likely linked to the fact that in Flores et al. (2006), we did not consider all possible ranges of size, PA, inclination, rotation velocity and RC gradient to derive this mean correction, as we were limited by hydro-dynamical models of spiral galaxies available to us at that time. Another difference is the exponential dependence of α with galaxy size found in Flores et al. (2006), which is not reproduced here. The reason for this is that in Flores et al. (2006), we used the same simulation of an Sbc galaxy to simulate distant galaxies having different sizes, which induced an intrinsic correlation between the RC gradient and the galaxy size. Our tests show that if we introduce this correlation in the Monte-Carlo simulations, we then recover the exponential variation of α with R_{half}.

The brightening found in the K-band TFR was not initially detected by Flores et al. (2006). In Fig. 8, we show the K-band TFR obtained following the Flores et al. (2006) method to correct ΔV_{obs}, i.e., applying a constant correction factor of 1.2. The black line shows the Verheijen (2001) K-band local TFR using V_{flat} as a kinematical tracer for the rotation velocity, i.e., the relation used as a local reference by Flores et al. (2006). Both the local and distant relation are then in good agreement: if we fix the slope of the distant relation to the local one, we find a shift $\sim$ 0.1 mag between the zero point of the distant and the local relations. Therefore, we retrieve the Flores et al. (2006) results that no significant evolution in zero point can be detected. The reason for such a difference is twofold.

First, as detailed in Hammer et al. (2007), we found a discrepancy between the K-band TFR derived in the Verheijen (2001) sample, compared to those derived in two other local samples (Courteau 1997; Pizagno et al. 2007). We show in Hammer et al. (2007) that this discrepancy is due to the larger fraction of faint and slow rotating galaxies in the Verheijen (2001) sample compared to the two other ones. Indeed, such galaxies have a larger gas fraction, which results in a different slope at the low-mass end of the TFR (McGaugh 2005). Recently, Noordermeer & Verheijen (2007) have derived a new K-band local TFR: they find a slope similar to the one inferred by Hammer et al. (2007) after restricting the Verheijen (2001) TFR to the high-mass end. However, in Flores et al. (2006), the relation used as a local reference was directly the Verheijen (2001) relation. If we re-fit the distant RD sub-sample using the rotation velocities derived following Flores et al. (2006), but now using the slope of the SDSS local relation (i.e., the one used in Fig. 7, see the blue lines in Fig. 8), we find a shift ~0.4 mag between the distant and the local zero points. Compared to Flores et al. (2006), we now use a different local sample which provides us with a better control of systematic effects that can occur in the comparison with the distant sample (see Sect. 4.2.2): this rigorous approach allows us to recover $\sim$ 60% of the TFR zero point shift, previously hidden by spurious effects.

Second, we have significantly improved the method for correcting the rotation velocity since the preliminary work of Flores et al. (2006). This is illustrated in Fig. 9, where we compare the rotation velocities derived following Flores et al. (2006) and those derived in this study: this figure reveals that Flores et al. (2006) underestimated the rotation velocity in RDs by 11% on average, which corresponds to a ~0.05 dex shift in $\log(V_{flat})$, or ~0.3 mag once converted into a M_K shift using Eq. 1. Therefore, we attribute the remaining ~40% of shift of the TFR zero point not previously detected to the improvement in the rotation velocity derivation.

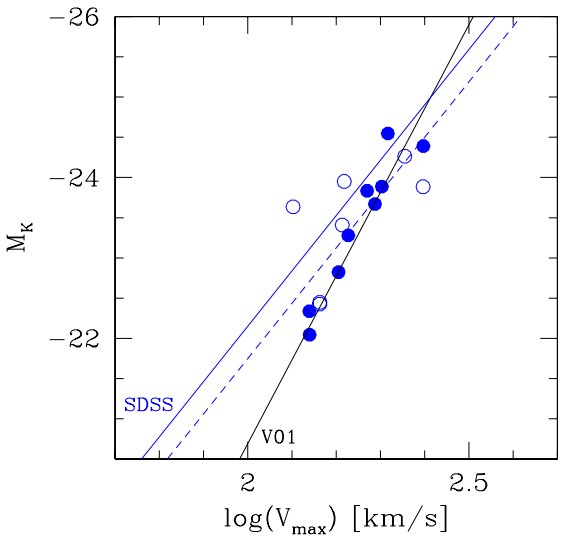

Fig. 8. K-band TFR derived following the Flores et al. (2006) methodology, for the RD sub-sample. The black line is the local relation of Verheijen (2001), i.e., the one used as a reference by Flores et al. (2006). Note that K-band magnitudes in the distant sample have been converted into the Vega system using $M_K(Vega) = M_K(AB) - 1.85$. For simplicity, we assume that the K' magnitudes of Verheijen (2001) are roughly equivalent to those derived in the distant sample using the ISAAC Ks filter. The blue dash line is the SDSS local TFR used as a reference in this study (converted into the Vega system). The blue dash line is a linear fit to the distant RDs, which has a zero point 0.34 mag lower than the local one, fixing the slope to the local value. Open symbols represent galaxies from the new CDFS sample, while full symbols represent galaxies used in Flores et al. (2006).

Finally, Fig. 8 provides us with a useful cross-check of the new method used in this study to correct the rotation velocity. Indeed, in Fig. 8, one RD (J033212.39-274353.6) seems to be relatively shifted to lower velocities compared to other distant rotating disks. This galaxy was already identified as having a particularly high α value in Sect. 3.3, while it falls well along the TFR in Fig. 7. This suggests that the new method of correction seems to be better suited for deriving rotation velocities: comparing Fig. 8 with Fig. 7, we note that the dispersion of the RD sub-sample is significantly reduced using the new method of correction.

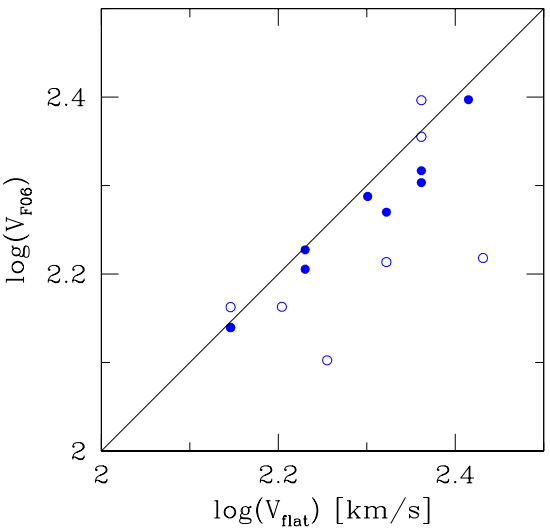

Fig. 9. Comparison between the rotation velocities V_{F06} obtained using the method of Flores et al. (2006) (i.e., a constant correction factor of 1.2) vs. rotation velocities V_{flat} derived using the new method used in this paper, for the sub-sample of RDs. V_{F06} underestimates V_{flat} by ∼11% on average. Open symbols represent galaxies from the new CDFS sample, while full symbols represent galaxies used in Flores et al. (2006).

5.2. Origin of the scatter in the distant relation

Using the spatially resolved kinematics provided by 3D spectroscopy, we confirm earlier results that all the dispersion of the distant relations can be explained by dynamically non-relaxed galaxies (Flores et al. 2006). These galaxies are found to be out of dynamical equilibrium, with an important contribution of random motions rather than ordered motions, especially among the most compact ones (Puech et al. 2006; Weiner et al. 2006). Ongoing comparisons between hydro-dynamical simulations of galaxy mergers with GIRAFFE data reveal that they could be associated with major mergers (Puech et al. 2007; Puech et al., in prep.). Such events provide us with a natural link between CK galaxies and morphologically peculiar galaxies (see Paper II), which cause an increase in the dispersion of the TFR at high redshift (Kassin et al. 2007; Atkinson et al. 2007).

On the other hand, it is still unclear whether or not more quiescent processes, such as secular gas accretion through internal processes (bars), or cold-gas flows (Dekel & Birnboim 2006; Keres et al. 2005), could explain such anomalous kinematics at relatively large spatial scales, especially for CK galaxies (see Paper I). More work is needed to compare dynamical predictions of such events with observations.

5.3. Comparison with the evolution of the K-band luminosity density

Finding a 0.66 mag *brightening* of the K-band TFR between $z \sim 0.6$ and $z = 0$ appears to be quite surprising, given the opposite trend seen in the evolution of the K-band luminosity density in "blue" galaxies over the same redshift range. Indeed, one may reasonably assume that "blue" star-forming galaxies and emission line galaxies belong to the same population (Hammer et al. 1997): Arnouts et al. (2007) find that the K-band luminosity density of blue star-forming galaxies *fades* by 0.5-0.6 mag from $z \sim 0.6$ to $z = 0$, which is exactly the opposite trend. What seems to be a clear contradiction actually simply reflects two very different methodologies.

As we have detailed above, the TFR allows us to compare two physically connected populations of galaxies, i.e., the local spirals and the distant rotating disks: the evolution of this relation directly reflects the evolution of the K-band luminosity in *rotating disks of same total mass* between $z \sim 0.6$ and $z = 0$, assuming that the rotation velocity can be used as a proxy for the total mass (Hammer et al. 2007). On the other hand, the color selection used to select "blue" galaxies at $z = 0$ and at $z \sim 0.6$ can lead to very heterogeneous galaxy populations when comparing their luminosity densities. Indeed, optical colors are well known to be seriously affected by instantaneous star formation and extinction. Actually, the evolution of the K-band luminosity density in "blue" galaxies simply reflects the number evolution of "blue" galaxies, which are much more numerous at high redshift (e.g., Ellis 1997).

To explicitly check that there is no contradiction between the evolution of the TFR zero point and the evolution of the K-band luminosity density, we have derived the K-band luminosity density in the complete GIRAFFE sample (i.e., including all dynamical classes). Indeed, as stated in Sect. 2.1, the GIRAFFE sample is representative of $z \sim 0.6$ emission line galaxies with $M_J(AB) \leq -20.3$ (i.e., with $M_{stellar} \geq 1.5 \times 10^{10} M_{\odot}$, see Paper I). We therefore expect a K-band luminosity density in this sample that represents well the luminosity density of "blue" galaxies at these redshifts. Indeed, we estimated the K-band luminosity in the GIRAFFE sample to be $\log(\rho_K) = 8.74$ $L_{\odot}.Mpc^{-3}$, which is in very good agreement with the K-band luminosity density of "blue" star-forming galaxies found by Arnouts et al. (2007). This comparison confirms that the GIRAFFE sample is well representative of $z \sim 0.6$ emission line galaxies: the K-band luminosity density in the GIRAFFE sample is consistent with the results inferred from studies using much larger samples.

5.4. Did distant rotating disks double their stellar-mass over the last 6 Gyr?

Once restricted to well-relaxed RDs, we find, between $z \sim 0.6$ and $z = 0$, a shift of the TFR zero point of 0.66±0.14 mag in M_K or -0.1±0.02 dex in $\log(V_{flat})$. We now turn to the interpretation of this shift in terms of galaxy evolution.

Could there be any so-called "progenitor bias" between distant RDs and local relaxed spirals, meaning that the latter would not be the descendants of the former? Indeed, local RDs are found to be two times more numerous than distant ones (see Paper II), which means that some of them were not in a relaxed dynamical state at $z \sim 0.6$ (being then PR or CK). However, local intermediate-mass spirals have only a low probability to have undergone a major merger since $z \sim 0.6$ (15-30%, as dis-

cussed in Puech et al. (2007)): this means that most distant RDs must dynamically evolve smoothly towards local relaxed spirals, which in turn implies that distant RDs are necessary the progenitors of a majority of local spirals. Therefore, it makes sense to interpret the evolution of the RD-restricted TFR as an evolution in luminosity, rotation velocity, or a combination of the two. Recall that in doing so, we assume no evolution in slope (see Sect. 4.1): a larger sample will be required to directly tackle the possible evolution is slope of the TFR and the details of the evolutionary path between distant and local RDs.

We first discuss the possibility that this shift would correspond to a pure luminosity brightening of 0.66±0.14 mag in RDs over the last 6 Gyr. Such a luminosity brightening in RDs would then correspond to a growth in stellar-mass, which can be estimated in the following way. Between $z \sim 0.6$ and $z = 0$, the evolution in $\log(M_{stellar}/L_K)$ is found to be ranging between 0.13 and 0.16 dex (Drory et al. 2004; Arnouts et al. 2007), depending on the selection criteria. Using $\log(M_{stellar}) = \log(M_{stellar}/L_K) + \log(L_K)$, one finally finds a stellar-mass evolution of 0.39-0.42 dex. A more exhaustive derivation, using the stellar-mass TFR, leads to a very similar conclusion, with an evolution in zero point of $0.36^{0.21}_{-0.06}$ dex between $z \sim 0.6$ and $z = 0$ (see Appendix A). On the other hand, the evolution of the cosmic stellar-mass density over the same redshift range is found to be ∼0.1-0.16 dex (Dickinson et al. 2003; Drory et al. 2004; Arnouts et al. 2007). Hammer et al. (2005) found that most of the present-day stellar-mass formed since $z = 1$ occur in intermediate-mass galaxies (see also Bell et al. 2005), which in turns include 60% of emission line galaxies at $z \sim 0.6$ (Hammer et al. 1997). Hence, if we assume that, on average, quiescent galaxies do not evolve in stellar-mass, one can estimate the growth in stellar-mass between $z \sim 0.6$ and $z = 0$ in intermediate-mass, emission line galaxies to be ∼0.32-0.38 dex. Therefore, this interpretation of the TFR zero point shift as a pure luminosity evolution is roughly in agreement with the evolution of the cosmic stellar-mass density over the same redshift range. Moreover, this interpretation is supported by the fact that distant RDs are found to be LIRGs or at least star-bursting, i.e., they are actively forming stars at very high rates (see Paper II).

Interpreted that way, the evolution of zero point of the K-band TFR simply reflects the growth in stellar-mass of the most active population over the last 6 Gyr, i.e. star-forming intermediate-mass galaxies, by a factor ∼2.5-2.6. Strikingly, this matches well the gaseous O/H phase abundance of $z \sim 0.6$ emission line galaxies, which is, on average, half that of present day spirals in the same range of stellar mass (Liang et al. 2006). Such an evolution in stellar-mass would imply that RDs have converted an important amount of gas into stars over the last 6 Gyr. In other words, the main evolutionary path for RDs during the last 6 Gyr would be conversion of gas into star through gas supply, which is further supported by their relatively low gas disk V/σ values (Puech et al. 2007) and the inside-out build-up of their stellar disks (see a detailed discussion in Paper II).

The opposite interpretation is that the shift of zero point of the K-band TFR would correspond to a pure rotation velocity evolution of -0.1±0.02 dex between $z \sim 0.6$ and $z = 0$. Even in this case, the observed evolution in $M_{stellar}/L_K$ over this redshift range still implies, on average, a substantial growth in stellar-mass of 0.13-0.16 dex in intermediate-mass galaxies (see above). As a consequence, the stellar-mass growth in *quiescent* intermediate-mass galaxies should be roughly the same, as the stellar-mass growth in the whole population (i.e., quiescent or not) is observed to be of that order of magnitude in this redshift range. This is clearly not what is observed, as ∼80% of the stellar-mass formed since z=1 occurred in star-forming galaxies (LIRGs, see Hammer et al. 2005). We can therefore rule out a pure evolution along the velocity axis.

The last possibility is a combined evolution along both axes, i.e. a simultaneous brightening in luminosity with a decrease in rotation velocity V_{rot}. According to the Virial theorem, V^2_{rot} scales as the ratio of the total mass enclosed within the optical radius R_{opt}, over R_{opt} ($\sim 3.2R_d$ in both distant and local galaxies, see Paper II). A decrease in V_{rot} between $z \sim 0.6$ and $z = 0$ would then imply a decrease of this ratio, which in turn would imply that R_{opt} (or R_d) increases faster than the total mass over the same redshift range. Between $z \sim 0.6$ and $z = 0$, R_d does not seem to evolve strongly, at least in the RD subsample (see Paper II; see also Puech et al. 2007). Therefore, only a very moderate increase of the total mass enclosed within R_{opt} could occur over this redshift range. Such a scenario could also be in agreement with observations: as stated above, local intermediate-mass spiral only have a low probability to have undergone a major merger since $z \sim 0.6$ (15-30%, see Puech et al. 2007 and references therein). Therefore, most distant RDs should be already mostly assembled at $z \sim 0.6$, and should not undergo strong evolution in terms of total-mass from $z \sim 0.6$ to $z = 0$.

As a very crude tentative to explore the real evolution along both axes, we compare our results with the model of spherical gas accretion of Birnboim et al. (2007). Indeed, Birnboim et al. (2007) present a model of accretion for a star-bursting galaxy at ∼0.7 and describe its subsequent evolution in terms of mass, down to $z = 0$. Although it is not clear whether or not such a model could be representative of all the properties of distant RDs, we will assume that it can be use to constrain the average mass evolution in a typical RD halo. In that case, Birnboim et al. (2007) results would suggest that the baryonic mass in the disk would remain constant between $z \sim 0.6$ and $z = 0$, while the *Virial* baryonic mass would roughly double (see their Fig. 2). On the other hand, Conroy et al. (2007) found that the Virial-to-stellar mass ratio in intermediate-mass galaxies is roughly constant between $z = 1$ and $z = 0$. Assuming that the sub-sample of RDs follows the same trend, one can combine the Conroy et al. (2007) observational results with the model of Birnboim et al. (2007), and find that RDs would roughly double their stellar-mass between $z \sim 0.6$ and $z = 0$. Accounting for the evolution in mass-to-light ratio over this redshift range (see above), this would translate into an evolution of 0.35-0.43 mag in luminosity, to be compared to the 0.66 mag found in the evolution of the TFR zero point. Once translated into $\log(V_{flat})$, this would roughly let us with a -0.04 dex evolution along the velocity axis, between $z \sim 0.6$ and $z = 0$.

In conclusion, we find that the most likely interpretation of the evolution of the TFR zero point is the one where this shift reflects mostly a luminosity evolution of RDs. We estimated

a very rough upper limit on the contribution of an evolution along the velocity axis to be at most one half of the total shift of zero point. Such a brightening of distant RDs over the last 6 Gyr would indicate a doubling of their stellar-mass, which is independently supported by their other dynamical and morphological properties.

Finally, this could suggest that the *baryonic* (stars *plus* gas) TFR would not evolve with redshift: if one accounts for the (average) two times larger gas fraction of $z \sim 0.6$ galaxies compared to $z = 0$ (Liang et al. 2006), one finds that distant galaxies roughly fall back onto the local smTFR (see Appendix A). Indeed, studies of the local baryonic TFR have shown that galaxies having $V_{flat} \leq$100 km/s systematically fall below the TFR defined by more massive galaxies (e.g., McGaugh 2005). However, once the gas fraction is accounted for, all galaxies follow the same *baryonic* TFR. Interpreted that way, our results simply suggest an evolution of this threshold toward higher masses (velocities) at higher redshifts, being at least $V_{flat} \sim$300 km/s at $z \sim 0.6$. This supports the idea that the baryonic TFR would be much more 'fundamental" that the stellar-mass TFR (McGaugh 2005).

6. Conclusion

We have studied the evolution of the K-band TFR, using a representative sample of 65 emission line, intermediate-mass galaxies at $z \sim 0.6$, unaffected by field-to-field variations within Poisson statistics, and observed using 3D spectroscopy. We have presented and tested a new method allowing us to safely recover V_{flat} of distant galaxies. We have also largely investigated possible sources of systematic effects, which can be particularly important when studying the evolution of the TFR. We have particularly paid attention to analyze both the local and distant samples in as similar as possible ways. We draw the following conclusions:

(1) All the enlarged dispersion of the distant TFR is caused by galaxies with anomalous kinematics, ranging from perturbed rotators to very dynamically disturbed galaxies. We find a positive and strong correlation between the complexity of the kinematics and the scatter contributed to the TF. Once restricted to relaxed rotating disks, the TFR seems to not have evolved in scatter, which also might suggest no evolution in slope;

(2) We detect for the first time a significant evolution of the K-band TFR zero point, which we attribute to an average brightening of $z \sim 0.6$ galaxies by 0.66±0.14 mag. We attribute this evolution to the fact that selected distant galaxies are either star-bursts or LIRGs. The distant emission line rotating disks represent roughly one fourth to one fifth of present-day spiral progenitors, and one half of the whole population of $z \sim 0.6$ intermediate-mass rotating disks (see Paper II). Therefore, a significant part of spiral progenitors are doubling their stellar masses during the last ~6 Gyr, in good agreement with former studies on the evolution of the mass-metallicity relation (Liang et al. 2006), which would suggest no evolution of the baryonic TFR with redshift;

(3) Current studies of the evolution of the TFR, even using spatially resolved kinematics, are still limited by important systematic uncertainties, which can be attributed to the limited spatial resolution of the kinematics, and to the derivation of the stellar-mass. These systematic uncertainties represent 20% of the evolution in zero point of the K-band TFR.

Further progress in the study of the evolution of the TFR will benefit from a forthcoming larger sample of RDs. This will allow us to reduce the random uncertainties, let the slope free during the fit, and start studying TF residuals. Moreover, although we have limited the local sample to galaxies having a well defined rotation curve, a decisive answer about the evolution of the TFR will need both local and distant representative samples treated all the same way, from the observational strategy (3D spectroscopy) to the data analysis itself, as we did in this paper. A similar analysis in a representative local sample observed *using 3D spectroscopy* will be needed to confirm the above results. This point will be addressed in a future study, using the local kinematic GHASP survey, whose analysis is currently on-going (Epinat et al. 2008). Finally, an important limitation remains linked to systematic uncertainties, which are mostly due to a lack of spatial resolution. The only way to overcome the former will be to develop a new generation of optical integral field spectrographs with higher spatial resolution, i.e., assisted by adaptive optics. In this respect, the future extremely large telescopes will allow us to make a decisive leap forward in our understanding of the TFR (Puech et al. 2008).

Appendix A: The evolution of the stellar-mass TFR

A.1. The local stellar-mass TFR

Stellar masses $M_{stellar}$ were estimated from $M_{stellar}/L_K$ ratios using the method of Bell et al. (2003). To do this, we used a solar luminosity in the Ks-band of 3.28 (Vega) and assumed a "diet" Salpeter IMF (Bell et al. 2003). This method makes advantage of the tight correlation found between rest-frame optical colors and $M_{stellar}/L_K$ ratios, assuming a universal IMF. These correlations are found to be relatively insensitive to the details of galaxy SFH, dust content, and metallicity (Bell & de Jong 2001; Bell et al. 2003), which makes them pretty useful for deriving the stellar-mass without relying too strongly on the details of the stellar population synthesis. Note that following this method, $M_{stellar}/L_K$ ratios are corrected for the amount of light due to red giant stars using g-r colors.

According to Bell et al. (2003), using this method, the total random uncertainty on $\log(M_{stellar}/M_{\odot})$ at $z \sim 0$ should be lower than 0.1 dex, and the systematic uncertainties due to galaxy ages, dust, or bursts of star-formation can reach 0.1 dex. Finally, the influence of TP-AGB stars in the derivation of stellar-masses could result in an over-estimation of the stellar-mass by ~0.14 dex (Maraston et al. 2006; Pozzetti et al. 2007) in a systematic way.

Using this method, we converted the local K-band TFR in the sub-sample of the SDSS (see Sect. 2.2) into stellar masses and found:

$$\log(M_{stellar}/M_{\odot}) = 4.46 \pm 0.53 + (2.8 \pm 0.23) \times \log(V_{flat}), \quad (A.1)$$

with σ_{res}=0.15 dex.

A.2. The distant stellar-mass TFR

To estimate stellar-masses in the distant sample (see Tab. 1), we used the same method as in the local sample, i.e., the K-band luminosity and B-V rest-frame colors. One important issue is whether or not the same correlations between color and $M_{stellar}/L_K$ ratios found at z=0 by Bell et al. (2003) can be directly applied at higher redshift: Borch et al. (2006) show that it seems to be indeed the case at least up to z∼0.6 (see their Fig. 4), with an associated random uncertainty of ∼0.3 dex, and an average systematic uncertainty of up to -0.2 dex (i.e., towards an overestimation of the stellar-mass at high z).

We show the derived distant smTFR in Fig. A.1. The smTFR shows the same trend with the kinematic classification that the K-band TFR. Restricting to RDs, and holding again the slope constant, the distant and local relations have similar dispersions (σ_{res}=0.12 dex). If we let the slope free during the fit, we also find a residual dispersion of 0.12 dex, suggesting again that assuming no evolution in slope is acceptable. Holding the slope to the local value, the distant smTFR zero point is found to be 4.10±0.16(random)$^{+0}_{-0.2}$(systematic, see above), i.e., 0.36 dex smaller than the local zero point (see Tab. A.1). A Welcher's t-test gives a probability ≪1% that the two relations have the same zero point.

A.3. Stellar-mass systematic uncertainties

The most important systematic uncertainty is certainly the one associated with mass-to-light ratios [M/L] predicted by stellar population synthesis [SPS] models. Absolute values of M/L depends mostly on the SPS model and IMF used, and more particularly on the prescriptions for the TP-AGB stellar evolution phase (Maraston 2005; Maraston et al. 2006)): Pozzetti et al. (2007) have compared M/L predictions between Bruzual & Charlot (2003) and Maraston (2005) SPS models and found a systematic difference of -0.14 dex due to different prescriptions for TP-AGB stars. However, they found that this systematic is constant with redshift, at least up to $z \sim 1.2$. In other words, at a given IMF, relative predictions between two different redshifts of SPS models are much more robust in terms of M/L predictions.

We therefore focus in Fig. A.2 on the evolution of $\log(M_{stellar}/L_K)$ between $z \sim 0.6$ and $z = 0$: we show the histograms of $\log(M_{stellar}/L_K)$ derived using the Bell et al. (2003) method, both in the distant and local samples. Both histograms have been centered using the median $\log(M_{stellar}/L_K)$ of the local sample: we find that $\log(M_{stellar}/L_K)$ evolves from $z \sim 0.6$ to $z = 0$ by ∼0.06 dex. In this figure, we also show other determinations of the evolution of $\log(M_{stellar}/L_K)$ from the literature. Drory et al. (2004), using Maraston (1998) SPS models,

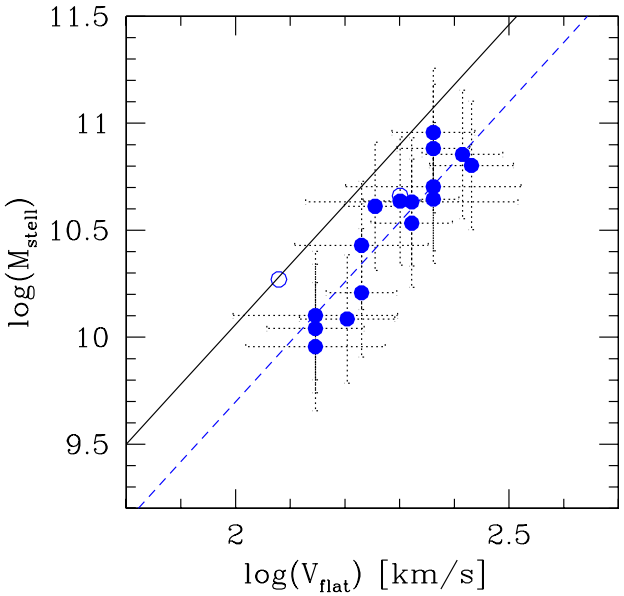

Fig. A.1. Evolution of the stellar-mass TFR in the RD subsample (the two RD+ galaxies are represented with open blue dots). The black line is the local smTFR, while the blue dashline represent a linear fit to the $z \sim 0.6$ smTFR

found an evolution of 0.13 dex in galaxies with stellar masses between $4\times10^{10}M_{\odot}$ and $10^{11}M_{\odot}$, i.e., in a range of stellar-mass similar to GIRAFFE galaxies. This is similar to the 0.15 dex evolution found by Arnouts et al. (2007) in a flux-limited sample over the same redshift range, using Bruzual & Charlot (2003) SPS models. Furthermore, Arnouts et al. (2007) find an evolution of 0.16 dex once restricted to a sample of blue star-forming galaxies. Because such blue galaxies and emission line galaxies probably belong to the same populations (Hammer et al. 1997), we conclude that we might be underestimating the evolution of $\log(M_{stellar}/L_K)$ by up to ∼0.16-0.06=0.1 dex in a systematic way.

What is the origin of this systematic effect? As $\log(M_{stellar}/L_K)$ mostly depends on color and not on mass, Bell et al. (2003) used SPS models to predict their "average" correlations given a reasonable range of SPS parameters (e.g., metallicity, star formation histories). However, Bell et al. (2003) did not explicitly fit the age but assumed instead a reference age of 12 Gyr at $z = 0$. This introduces a systematic difference with other results where age is fitted explicitly. For instance, Drory et al. (2004) find an average age of 8.1 Gyr at $z = 0$. If one compares the median $\log(M_{stellar}/L_K)$ found in the local SDSS sample used in this study, with the average value found by Drory et al. (2004) in a similar mass range, one finds a difference of -0.08 dex (which accounts for the different IMF used). Similarly, we find a difference of -0.16 dex between the median $\log(M_{stellar}/L_K)$ found in the GIRAFFE sample, and the average value found by Drory et al. (2004) at $z = 0.6$. Noteworthy, these values are consistent with the systematic error-bars quoted above. Moreover, they suggest that we un-

Table A.1. Fits to the local and distant smTFRs, using $\log(M_{stellar}/M_{\odot}) = a + b \times \log(V_{flat})$.

K-band TFR	Slope a	Zero point b	Comments
Local relation	2.8±0.23	4.46±0.53	SDSS sub-sample
Distant RDs	2.8	4.10±0.16	Using local slope
Distant RDs	3.28±1.10	3.01±2.47	Slope free
Distant RD/RD+	2.8	4.13±0.15	Using local slope
Distant RD/RD+	2.61±1.33	4.56±3.03	Slope free

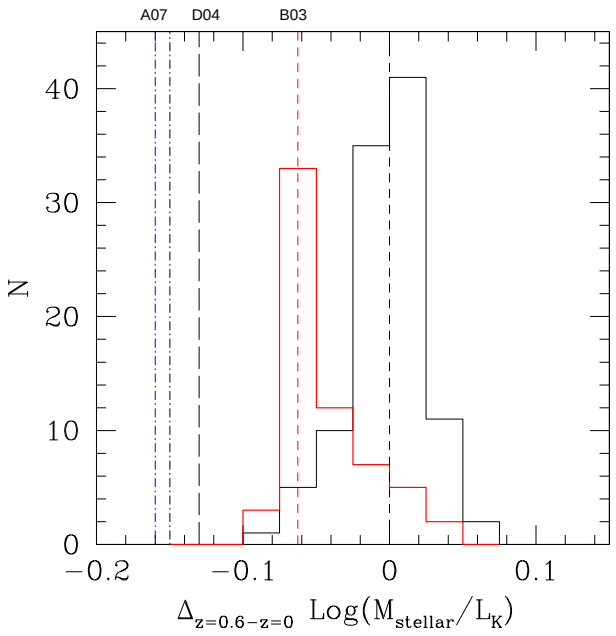

Fig. A.2. Histograms of $\log(M_{stellar}/L_K)$ found in the local and distant samples of galaxies using the method of Bell et al. (2003). Both histograms have been re-centered using the median found in the local samples, which allows us to directly infer the evolution of $\log(M_{stellar}/L_K)$ between $z \sim 0.6$ and $z = 0$, i.e., ∼0.625 dex. Also shown, the evolution of $\log(M_{stellar}/L_K)$ found by Drory et al. (2004) in a sample of intermediate-mass galaxies (black long-dashed line), and Arnouts et al. (2007) in blue star-forming galaxies (blue mixed-line) or independently of the color (black mixed-line).

derestimate the evolution of $\log(M_{stellar}/L_K)$ between $z = 0$ and $z \sim 0.6$ by -0.08 dex, which is consistent with Fig. A.2.

In summary, these comparisons show that we are probably underestimating the evolution of $\log(M_{stellar}/L_K)$ between $z = 0$ and $z \sim 0.6$ by -0.08 dex, and maybe up to -0.1 dex due to the use of the simplified prescriptions for M/L of Bell et al. (2003). This directly translates into a systematic effect of the evolution of smTFR zero point by up to +0.1 dex.

A.4. Total systematic uncertainty

We summarize all possible sources of systematic uncertainty identified so far in Tab. A.2. We expressed all of them in terms of their influence on the shift of zero point between the distant and the local smTFRs. Taking into account all these uncertainties, we find a shift of the smTFR zero point of $0.36^{0.21}_{-0.06}$ dex between $z \sim 0.6$ and $z = 0$. Systematic uncertainties represent up to ∼60% (in dex) of the evolution detected in zero point, i.e., much larger than systematic uncertainties affecting the evolution of the K-band TFR zero point. Indeed, the derivation of stellar-mass is highly model-dependent, which implies a large additional uncertainty. However, note that these effects tends to overestimate the stellar-mass at high redshift, i.e., to minimize the evolution of the smTFR. Using $\log(M_{stellar}/L_K) = \log(M_{stellar}) - \log(L_K)$, one finds that $\log(M_{stellar}/L_K)$ evolves by ∼0.1 dex ($= 0.36 - 0.66/2.5$) between $z \sim 0.6$ and $z = 0$ in the sub-sample of RDs. Therefore, the evolution in the zero point of the smTFR is quite robust, in the sense that we might have minimized the evolution of $M_{stellar}/L_K$ through the choice of the method used to derive the stellar-mass (see Sect. A.3).

Acknowledgements. We thank all the GIRAFFE team at the Observatories of Paris and Geneva, and ESO for this unique instrument.

References

Amram, P., Adami, C., Balkowski, C., et al. 2002, Ap&SS, 281, 393
Arnouts, S., Vandame, B., Benoist, C., et al. 2001, A&A, 379, 740
Arnouts, S., Walcher, C.J., Le Fèvre, O., et al. 2007, A&A, submitted, astro-ph/0705.2438
Atkinson, N., Conselice, C.J., & Fox, N. 2007, MNRAS, submitted, astro-ph/0712.1316
Bamford, S.P., Aragon-Salamanca, A., & Milvang-Jensen, B. 2006, MNRAS, 366, 308
Bell, E.F. & de Jong, R.S. 2001, ApJ, 550, 212
Barnes, J.E. 2002, MNRAS, 333, 481
Bell, E. F., McIntosh, D. H., Katz, N., & Weinberg, M. D. 2003, ApJS, 149, 289
Bell, E. F., Papovich, C., Wolf, C., et al. 2005, ApJ, 625, 23
Bell, E. F., Zheng, X.Z., Papovich, C., et al. 2007, ApJ, 663, 834
Birnboim, Y., Dekel, A., & Neisten, E. 2007, MNRAS, submitted, astro-ph/0703435
Blanton, M.R., Schlegel, D.J., Strauss, M.A., et al. 2005, AJ, 129, 2562
Böm, A., Ziegler, B.L., Saglia, R.P., et al. 2004, å, 420, 97
Böm, A., & Ziegler, B.L. 2007, ApJ, 668, 846
Borch, A., Meisenheimer, K., Bell, E.F., et al. 2006, A&A, 453, 869
Bruzual, G., & Charlot, S. 2003, MNRAS, 244, 1000

Table A.2. Identified systematic uncertainties that could impact the shift of zero point between the local and the distant smTFRs. Systematic uncertainties on V_{flat} have been converted into $M_{stellar}$ using Eq. A.1. Negative values tend to reduce the shift of zero point, while positive values have the opposite trend.

Description	Bias on $M_{stellar}$ (dex)	Comments
Photometry	∼0	Comparison EIS vs. ACS in the CDFS
M/L_K Evolution with z	+0.1	Following Sect. A.3
IMF Evolution with z	+0.05	Following van Dokkum (2007)
Velocity correction	±0.06	See Sect. 4.2.3
Total	-0.06/+0.21	

Carignan, C., Chemin, L., Huchtmeier, W.K., & Lockman, F.J. 2006, ApJ, 641, 109
Carpenter, J.M. 2001, AJ, 121, 2851
Chemin, L., Balkowski, C., Cayatte, V., et al. 2006, MNRAS, 366, 812
Chiu, K., Bamford, S.P., & Bunker, A. 2007, MNRAS, 377, 806
Conselice, C. J., Bundy, K., Ellis, R. S., Brichmann, J., Vogt, N. P., & Phillips, A. C. 2005, ApJ, 628, 160
Conroy, C., Prada, F., Newman, J.A., et al. 2007, ApJ, 654, 153
Courteau, S. 1997, AJ, 114, 2402
Davé, R. 2007, MNRAS, submitted, astro-ph/0710.0381
De Rijcke, S., Zeilinger, W.W., Hau, G.K.T., et al. 2007, ApJ, 659, 1172
Dekel, A., & Birnboim, Y. 2006, MNRAS, 368, 2
Dickinson, M., Papovich, C., Ferguson, H.C., et al. 2003, ApJ, 587, 25
Drory, N., Bender, R., Feulner, G., et al. 2003, ApJ, 595, 698
Drory, N., Bender, R., Feulner, G., et al. 2004, ApJ, 608, 742
Dutton, A.A., van den Bosch, F.C., Dekel, A., et al. 2007, ApJ, 654, 27
Ellis, R. 1997, ARA&A, 25, 389
Epinat, B., Amram, P., Marcelin, M., et al., MNRAS, submitted
Flores, H., Hammer, F., Puech, M., Amram, P., & Balkowski, C. 2006, A&A, 455, 107
Franceschini, A., Rodighiero, G., Cassata, P., et al. 2006, A&A, 453, 397
Governato, F., Willman, B., Mayer, L., Brooks, A., Stinson, G., Valenzuela, O., Wadsley, J., & Quinn, T. 2007, MNRAS, 374, 1479
Hammer, F., Flores, H., Lilly, S.J., et al. 1997, ApJ, 481, 49
Hammer, F., Gruel, N., Thuan, T.X., et al. 2001, ApJ, 550, 570
Hammer, F., Flores, H., Elbaz, D., Zheng, X. Z., Liang, Y. C., & Cesarsky, C. 2005, A&A, 430, 115
Hammer, F., Puech, M., Chemin, L., Flores, H., & Lehnert, M. 2007, ApJ, 662, 322
Hogg, D.W. 1999, astro-ph/9905116
Kannappan, S. J., & Barton, E. J. 2004, AJ, 127, 2694
Kassin, S.A., Weiner, B.J., Faber, S.M., et al. 2007, ApJ, 660, 35
Keres, D., Katz, N., Weinberg, D.H., & Davé R. 2005, MNRAS, 363, 2
Kroupa, P. 2001, MNRAS, 322, 231
Liang, Y.C., Hammer F., & Flores, H. 2006, A&A, 447, 113
Maraston, C. 1998, MNRAS, 300, 872
Maraston, C. 2005, MNRAS, 362, 799
Maraston, C., Daddi, E., Renzini, A., et al. 2006, ApJ, 652, 85
Mason, E., Kaufer, A., & Hainaut, O. 2007, ISAAC Instrument data reduction cookbook
McGaugh, S.S. 2005, ApJ, 632, 859
Mo, H.J., Mao, S., & White, D.M. 1998, MNRAS, 295, 319
Neichel, B., et al. 2008, A&A, submitted
Noordermeer, E. & Verheijen, M.A.W 2007, MNRAS, accepted, astro-ph/0708.2822
Okamoto, T., Eke, V.R., Frenk, C.S. & Jenkins, A. 2005, MNRAS, 363, 1299
Persic M. & Salucci P. 1991, ApJ, 368, 60
Persson, S.E., Murphy, D.C., Krzeminski, W., et al. 1998, AJ, 116, 2475
Pizagno, J., Prada, F., Weinberg, D.H., et al. 2007, AJ, 134, 945
Portinari, L., & Sommer-Larsen, J. 2007, MNRAS, 375, 913
Press, W.H. 2002, Numerical recipes in C++: the art of scientific computing, Cambridge University Press
Puech, M., Flores, H., Hammer, F., Lehnert, M.D. 2006, A&A, 455, 131
Puech, M., Hammer, F., Flores, H., Östlin, G., & Marquart, T. 2006b, A&A, 455, 119
Puech, M., Hammer, F., Lehnert, M. D., & Flores, H. 2007a, A&A, 466, 83
Puech, M., Hammer, F., Flores, H. et al. 2007, A&A, accepted, astro-ph/0711.0611
Puech, M., Flores, H., Lehnert, M.D., et al. 2008, MNRAS, submitted.
Pozzetti, L., Bolzonella, M., Lamareille, F., et al. 2007, A&A, 474, 443
Ravikumar, C. D., et al. 2007, A&A, 465, 1099
Robertson, B., Bullock, J. S., Cox, T. J., Di Matteo, T., Hernquist, L., Springel, V., & Yoshida, N. 2006, ApJ, 645, 986
Russell, D.G. 2004, ApJ, 607, 241
Saintonge, A., Masters, K.L., Marinoni, C., et al. 2007, å, submitted, astro-ph/0710.0760
Salpeter, E.E. 1955, ApJ, 121, 161
Simard, L., & Pritchet, C.J. 1998, ApJ, 505, 96
Tully, R., & Fisher, J. 1977, A&A54, 661
Tully, R., & Fouqué, P. 1985 ApJS58, 67.
Tully, R., Pierce, M.J., Huang, J., et al. 1998, AJ115, 2264
van der Wel, A., Holden, B.P., Franx, M., et al. 2007, submitted, astro-ph/0707.2787
van Dokkum, P.G. 2007, ApJ, submitted, astro-ph/0710.0875
Verheijen, M.A.W. 2001, ApJ, 563, 694
Vogt, N., Herter, T., Haynes, M.P., et al. 1993, ApJ, 415, 95

Vogt, N., Forbes, D.A., Philips, A.C., et al. 1996, ApJ, 465, 15
Vogt, N., Philips, A.C., Faber, S.M., et al. 1997, ApJ, 479, 121
Weiner, B. J., et al. 2006, ApJ, 653, 1027
Yang, Y., Flores, H., Hammer, F., et al. 2007, A&A, accepted, astro-ph/0711.2305